sciendo

ANNALS OF WEST UNIVERSITY OF TIMISOARA PHYSICS
Vol. LXV, 2023

DOI: 10.2478/awutp-2023-0010

THERMAL PERFORMANCE OF DOUBLE PASS SOLAR AIR COLLECTOR: NUMERICAL AND EXPERIMENTAL INVESTIGATION

Yousef Belloufi[1,2], Amar Rouag*[3,4], Faris Aissaoui[2,5], Abdelmoumene-Hakim Benmachiche[6], Abdelhfid Brima[1]

[1]*Univerité Kadi Merbah Ouargla, Faculté Des Hydrocarbures, Département De Forage Et Mécanique Des Chantiers Pétroliers BP 511 Ouargla 30000, Algeria.*
[2] *Laboratoire de Génie Mécanique, LGM, Université de Biskra, B.P.145 R.P. 07000 Biskra, Alegria.*
[3]*Univerité Kadi Merbah Ouargla, Faculté Des Hydrocarbures, Département Des Energies Renouvelables, BP 511 Ouargla 30000, Algeria.*
[4]*Laboratoire de Génie Energétique et Matériaux (LGEM), Université Mohamed Khider Biskra, B.P.145 R.P. 07000 Biskra, Alegria.*
[5]*Université de Ghardia, Faculté des Science et de la Technoogie, Département D'automatique et D'éléctomécanique 47000, Algeria.*
[6] *Département de Physique, Université de Batna, Algria.*
[*] *Corresponding author, Email address: rouag.amar@univ-ouargla.dz*

Article Info	Abstract
Received:01.08.2023 *Accepted: 25.10.2023* **Keywords:** Solar air heater, Double pass, Thermal performance, Experimental, Numerical	In this research study, the development of a theoretical model to estimate the efficiency of a double pass solar air heater (DPSAH) was the main objective. The mathematical model was compared to experimental results and found to be in agreement, both qualitatively and quantitatively. The model used energy balance equations to determine the outlet temperature and could solve the temperature equations of each component of the heater simultaneously. A matrix inversion method was used for this purpose. The study found that increasing the Nusselt number led to an increase in energy efficiency, but also caused a drop in outlet temperature at any solar radiation. The mass flow rate (MFR), with larger flow rates resulting in better efficiencies, had a significant impact on the double pass air heater's efficiency. Thus, increasing of DPSAH's length increases its thermal performances and reach its maximum values for L=9m. These findings could be beneficial in selecting the most efficient design parameters for DPSAH.

1. Introduction

Solar thermal energy has the potential to be utilized for the purpose of generating heat in domestic, industrial, and commercial settings. In addition to space heating in buildings and

process heat in industrial applications, it can be utilized to supply hot water for home usage. Solar collectors are employed in solar thermal heating systems to capture sunlight and transform it into heat. A flat, insulated box with a cover glass and an absorber plate within is the most typical style of solar collector used for heating. Sunlight is collected by the absorber plate and transformed into heat. After that, the heat is transferred to a fluid that passes through the heater, such as water or antifreeze. The heated fluid is then either used directly for space heating or domestic hot water or stored in a thermal storage tank for later use. In some cases, a backup heating system, such as a gas or electric boiler, is also installed to ensure a constant supply of hot water or space heating. Solar thermal heating system can be installed in new or existing buildings, and they can be designed to meet a range of heating needs. They are particularly well-suited for buildings located in areas with high levels of solar irradiance and can be an effective way to energy costs and greenhouses gas emissions associated with heating.

In the context of the global emphasis on switching to environmentally friendly energy sources, solar thermal energy systems can be employed with solar air heaters (SAHs) for some functions such as building heating, food drying, desalination, and air conditioning.[1] Solar air collectors were utilized as the primary component in a variety of solar drying systems for agricultural commodities. [2] Traditional solar air heaters have inherent drawbacks in terms of reduced thermal efficiency. A variety of solar air collector configurations have been created in an effort to find the best design for various purposes. Numerous solar collector designs have been suggested, among which are multi-pass solar collectors. Wijeysundes et al. [3] looked at the thermal efficiency of a solar heaters with two glazing options: single and double . They came to the conclusion that a double pass heater performs better than a single pass collector. The cost and performance analysis of double and triple pass solar air heaters has been studied by Choudhury et al. [4, 5]. Choudhury et al. [4] discovered that the double-pass solar air collector with a single cover had the best cost-effectiveness in comparison to the other designs based on their results. Additionally, the work of Chdhoury et al. [5] focused on examining the theoretical models of triple solar air collectors that had both single and double covers. They compared the performance of these solar air heaters with single pass air collectors that lacked a cover, as well as those with single and covers. The outcomes were presented as different design curves.. Mohamed [6] reported that te thermal efficiency of the conventional solar air collector can be improved by 18% by using a traditional double pass air collector, which he referred to as a counter-current sun collector. The study also suggested adding an extra fan power of 2 to 3W, which is not a significant amount. Singh [7] conducted an experimental and theoretical research on the different fin configuration of DPSAH, including inline, staggered,

and hybrid, with the aim of improving its thermal performance. They varied the geometrical parameters of the fin configuration and from 30. To 90, length and height of 0.007 to 0.028, and hydraulic diameter of 0.029 and 0.057 meters, using a range of Re=3000 to 24000. Experimental results demonstrated that a DPSAH (counter flow) had superior thermal performance over a single air pass. Shorter length fins were discovered to produce better outcomes in the hybrid staggered configuration. 3.8% was about how well hybrid staggered fins performed numerically in terms of heat transfer. Salih et al. [8] performed an experimental investigation on a trapezoidal (DPSAHs) utilizing both forced and natural air circulation. By incorporating trapezoidal fins on both sides of the absorber plate, the goal was to improve the thermal performance of the solar air collector. The study examined how solar irradiance and MFR impacted the performance of the DPSAH. The results showed that for forced air circulation, the highest efficiency was 64% and for natural air circulation, 73.5%. In addition, the MFR of air for forced convection was around three times higher than that for natural convection. Amit Kumar et al. [9] proposed a unique design for a DPSAH with a counter-flow, curved configuration. They carried out a quantitative investigation of the performance characteristics of this design under various flow and geometric conditions and compared it with several parallel designs. The findings suggested that the counter flow curved DPSAH with symmetrically arranged turbulators performed better than other designs in terms of thermal efficiency. With this arrangement, the thermal performance went up by as much as 23%. Sophian et al. [10] developed an unsteady-state mathematical model that incorporates unsteady energy balance equations for DPSAHs utilizing both porous and nonporous media. Their outcomes demonstrated that the thermal efficiency of DPSAHs with porous media usually ranges from 60.0% to 70.0%. Furthermore, Sopian et al. [11] investigated the effects of changes in the upper and bottom channel depth on the thermal efficiency of DPSAHs with porous media under different operating conditions, resulting in the creation of a steady-state mathematical model. Another approach to substantially improve collector efficiency is by increasing the heat transfer area, which can be accomplished through the use of corrugated surfaces [12] and finned absorbers [13-17]. In order to calculate the coefficients for local convective heat transfer, a number of experimental and numerical investigations have been taken into account. For instance, Saboya and sparrow [18]and Yoo et al. [19] measured the local coefficients in the heat exchangers using a naphthalene sublimation method. One of the methods most frequently used to calculate these coefficients is the inverse problems of heat conduction. The local heat transfer coefficient over finned-tube heat exchangers were ascertained by Hung et al. [20] and Benmachiche et al. [21] using the conjugate gradient

approach, which is based on the inversed algorithm scheme. The convective heat transfer coefficient in SAHs have been the subject of more investigation. In flat plate SAHs with rectangular plate fins positioned perpendicular to the flow, Moummi et al. [22] proposed a method for estimating these coefficients and compared the results with those obtained from a collector without fins. Aissaoui et al. [23, 24] conducted both experimental and theoretical research to simulate the local heat transfer coefficients in a single-pass flat plate SAH that operates under forced convection. They compared the theoretical predictions to measured temperatures under various solar radiation intensities.

Based on the above literature review, it is evident that prior investigations primarily relied on intricate models, while empirical studies on double pass solar air collectors are scarce. This study aims to address this gap by proposing a novel modeling approach, which involves partitioning the solar air heater into discrete differential segments within the collector. Next, as for the second objective of this research, we experimentally determined the local convective heat transfer coefficient using the recorded temperatures of the cover glass, absorber, fluid flow, and bottom plate as a baseline. The temperature distribution in the SAH was then predicted using these coefficients via a mathematical model derived from the system's energy balances. Different sun radiation intensities are used to compare the measured and projected temperature distributions. The findings of this research will undoubtedly receive strong support by enhancing future iterations of this collector through the development of improved models.

2. Mathematical model

This study focuses on examining a DPSAH. The research involves developing a mathematical model that utilizes energy balance equations (EBEs) for each component of the SAH system depicted in Figures (1, 2). To analyze the system, EBES are applied to individual elements treated as control volumes. Within each control volume, it is assumed that the air temperature varies linearly. This assumption holds true for relatively small collectors, specifically those with lengths less than 10 meters.

Subsequently, the average air temperature is calculated as: $T_f=(T_{f,i}+T_{f,o})/2$

The temperature distribution within various components of the collector, including the fluid flow, is determined through the use of (EBEs). These equations serve as a fundamental tool for heat transfer analysis and are specifically applied to a control volume of differential length. This control volume is oriented in parallel to the flow direction and is located on both the top plate of the glass cover and the absorber plate within the collector system. This

configuration, illustrated in Figure 1, enables a comprehensive examination of how heat is exchanged and distributed within the collector.

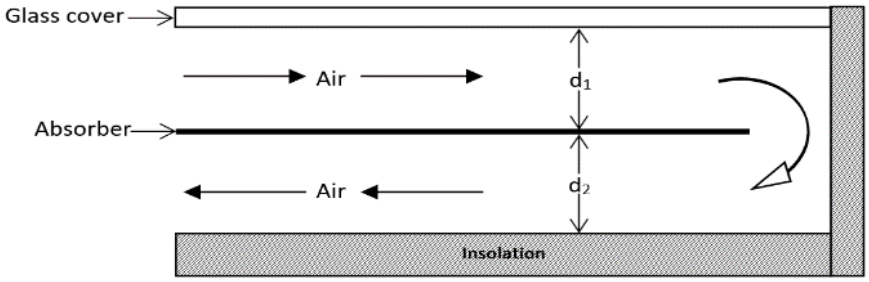


Figure 1. Schematic representation of the DPSAH model under study

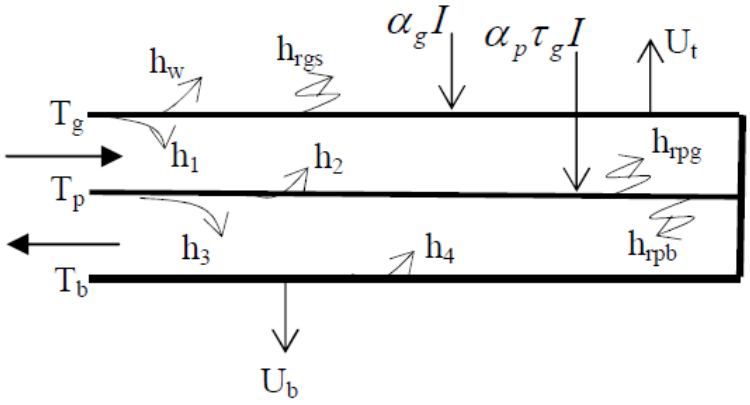


Figure 2. Schematic representation of heat transfer coefficients in DPSAH

2.1. Simplifying assumptions

In order to simplify the theoretical model, several assumptions have been made:

- The system is assumed to operate under steady-state conditions.
- Only the direction of the air flow is considered to affect the fluid's (air's) temperature.
- Heat transfer through the glass cover and absorber is considered to be one-dimensional and occurs perpendicular to the direction of the fluid flow.
- Negligible heat losses are expected from the lateral walls due to their small surface area.

2.2. Energy balances equations

The energy balances equations can be used to model the performance of various collector components, such as the absorber, bottom plate, glass cover and heat transfer fluid. By solving the equations, designers can optimize the performance of the heater components to maximize the efficiency of the solar thermal system.

EBEs have been written for each component (glass temperature T_1 , air flow 1 temperturT_{f1} , absorber plate temperature T_2 , air flow 2 temperature T_{f2} and absorber plate temperature T_2) of the collector within the control volume [13-15, 25, 26]:

a. Glass cover

The energy balance for the glass is expressed by the following equation [15, 16].

$$S_1 + h_{r21}(T_2 - T_1) + h_1(T_{f1} - T_1) + U_L(T_a - T_1) = 0 \quad , S_1 = \alpha_1 I_g$$

$$(h_{r21} + h_1 + U_L)T_1 - h_1 T_{f1} - h_{r21} T_2 = S_1 + U_L T_a \tag{1}$$

Where h_1, h_{r21}, α_1, U_L, T_a, are the convective heat transfer coefficient between glass cover and air flow, radiation heat transfer coefficients between glass cover and absorber plate, abrober plate emissivity, top heat loss coefficient and ambient temperature, respectively.

b. First air flow

The energy balance for the first fluid (f1) flowing in the upper channel is given by the following equation [15, 16].

$$\dot{m} C_p \frac{dT_{f1}}{w\,dx} = h_1(T_1 - T_{f1}) + h_2(T_2 - T_{f1})$$

$$\Gamma_1\left(T_{f1,i} - T_{f,i-1}\right) = h_1(T_1 - T_{f1}) + h_2(T_2 - T_{f1}), \quad \dot{m} C_p \frac{dT_f}{w\,dx} = \Gamma_1\left(T_{f1,i} - T_{f1,i-1}\right)$$

$$h_1 T_1 - (h_1 + h_2 + \Gamma_1) T_{f1} + h_2 T_2 = -\Gamma_1 T_{f,i-1} \tag{2}$$

Where $\dot{m}$, C_p and h_2 are respectively the mass flow rate of the fluid in the channel, specific heat capacity and convective heat transfer coefficient between absorber plate and the first air flow.

c. Absorber plate

The energy balance for the absorber is expressed by the following equation[15, 16].

$$h_2(T_2 - T_{f1}) + h_3(T_2 - T_{f1}) + h_{r21}(T_2 - T_1) + h_{r32}(T_2 - T_3) = S_2, \quad S_2 = \tau\alpha_2 I_g$$

$$-h_{r21} T_1 - (h_3 + h_3) T_{f1} + (h_2 + h_3 + h_{r32} + h_{r21}) T_2 - h_{r32} T_3 = S_2 \tag{3}$$

α_2 is the absorber absorption coefficient and τ is the glass transmittance.

d. Second air flow

The energy balance for the second fluid (f2) flowing in the lower channel is given by the following equation[15, 16].

$$\dot{m} C_p \frac{dT_{f2}}{w\,dx} = h_3(T_2 - T_{f2}) + h_4(T_3 - T_{f2})$$

$$\boldsymbol{\Gamma}_2\left(T_{f2,i} - T_{f2,i-1}\right) = h_3(T_2 - T_f) + h_4(T_3 - T_f)\,, \quad \dot{m}C_p\frac{dT_f}{w\,dx} = \boldsymbol{\Gamma}_2\left(T_{f,i} - T_{f,i-1}\right)$$

$$h_3T_2 - (h_3 + h_4 + \boldsymbol{\Gamma}_1)\,T_{f2,i} + h_4T_3 = -\boldsymbol{\Gamma}_2T_{f2,i-1} \tag{4}$$

In the equation 4, h_3 is the convective heat transfer coefficient between absorber plate and air flow and h_4 represents the convective heat transfer coefficient between bottom plate and air flow.

e. Bottom plate

Similarly, the energy balance for the insulation is given by the following[15, 16].

$$h_4\,(T_3 - T_f) + U_b\,(T_3 - T_a) + h_{r32}\,(T_3 - T_2) = 0$$

$$-h_{r32}T_2 - h_4T_{f2} + (h_{r32} + U_b + h_4)\,T_3 = U_bT_a \tag{5}$$

Where U_b is the overall thermal loss coefficient and h_{r32} is the radiation heat transfer coefficient between bottom plate and absorber plate.

2.3. Approximating the coefficients of heat transfer

Heat transfer coefficients can be can be estimated using a variety of methods, depending on the specific application and the type of heat transfer mechanism involved. The choice of method used to estimate the heat transfer coefficients will depend on the specific application and the available resources.

2.3.1. Influence of air currents

In order to determine the convective coefficient on the exterior surface, the following correlation is used [27] :

$$H_w = 5.7 + .8V \tag{6}$$

The air and absorber plate's convective heat transfer coefficient: equations (7) and (8) are used, respectively, [28, 29] to get the convective heat transfer coefficient for laminar and turbulent flow inside rectangular channels.

$$Nu = \frac{h_3\,D_{\mathrm{h}}}{k_f} = 4.4 + \frac{0.00398(0.7ReD_{\mathrm{h}}/L)^{1.66}}{1+0.0114(0.7ReD_{\mathrm{h}}/L)^{1.12}} \tag{7}$$

$$Nu = \frac{h_3D_h}{k_f} = 0.0158\,Re^{0.8} \tag{8}$$

Thermal energy transfer through electromagnetic waves: The absorber plate's solar radiation absorption is:

$$S_1 = \alpha . G \tag{10}$$

Radiative heat transfer coefficient between the sky and the cover glass: The coefficient of radiative heat transfer between the glass and the sky can be expressed using the equation:

$$h_{rs} = \frac{\sigma\, \varepsilon_1 (T_1 + T_s)(T_1^2 + T_s^2)(T_1 - T_s)}{(T_1 - T_a)} \tag{11}$$

The formula can be used to determine the temperature of the sky [30] :

$$T_s = 0.0552\, Ta^{1.5} \tag{12}$$

Coefficient of heat transfer by radiation between the absorber plate and the cover glass: equation (13) can be used to determine the coefficient of radiative heat transfer between cover glass and absorber plate:

$$h_{r21} = \frac{\sigma(T_1^2 + T_2^2)(T1 + T2)}{\frac{1}{\varepsilon_1} + \frac{1}{\varepsilon_2} - 1} \tag{13}$$

Coefficient of radiative heat transfer between the absorber and the lower plate. The coefficient of radiative heat transfer between the absorber and the lower plate can be calculated using the equation:

$$h_{r23} = \frac{\sigma(T_2^2 + T_3^2)(T2 + T3)}{\frac{1}{\varepsilon_2} + \frac{1}{\varepsilon_3} - 1} \tag{14}$$

Coefficient of thermal heat loss towards the back of the collector: the coefficient of thermal heat loss towards the back of the solar heater air can be calculated using the equation:

$$U_b = \frac{1}{i = \sum_1^n \frac{X_{bi}}{k_{bi}} + \frac{1}{h_w}} \tag{15}$$

Thermal loss coefficient for the front of the heater: the thermal loss coefficient for the air in front of the SAH is expressed as:

$$U_L = h_w + h_{rs} \tag{16}$$

2.4. Proprieties of air flow

The expressions below are used to represent the varying thermal properties of air [31]: Where

$$C_p = 999.2+0.143T_f+1.61\times10^{-4}\ T_f^2 -6.75\times10^{-8}\ T_f^3 \tag{17}$$

$$K=0.0244+0.6773\times10^{-4}T_f \tag{18}$$

$$\upsilon =0.12844\times10^{-4}+0.00105\times10^{-4}T_f \tag{19}$$

$$\rho= \frac{353.44}{T_f+273.15} \tag{20}$$

The air temperature, evaluated in Celsius, can be denoted as T_f.

2. 5. Solution method

In the context of a DPSAH, the difference method can be applied to approximate the fluid temperature gradient within a control volume of the collector. The temperature gradient is an important factor in the performance of the heater, as it affects the efficiency of heat transfer from the fluid to the collector surface. The difference method involves dividing the temperature difference between two adjacent points in the control volume by the distance between those points. In the case of a DPSAH, this might involve dividing the temperature difference between the inlet and outlet air streams by the distance between those two points. By applying this method at different points within the control volume of the DPSAH, an approximation of the temperature gradient across the collector can be obtained. This information can be used to optimize the design and operation of the collector to maximize its efficiency.

It's worth noting that the temperature gradient within a DPSAH can be influenced by many factors, including the geometry of the collector, the MFR, and the thermal properties of the materials used. Therefore, accurate modeling of the temperature gradient is important for predicting the performance of the heater and optimizing its design.

The temperature gradient of the air in each control volume is approximated using the difference method, which is expressed as:

$$\frac{dT_f}{dx} \approx \frac{T_{f,i}-T_{f,i-1}}{\Delta x} \tag{21}$$

The system of equations, which consists of 5 equations for the unknowns T_1, T_2, T_3, T_{f1}, and T_{f2}, is expressed in matrix form with a 5 × 5 matrix. Since the coefficient matrix is dependent on temperature, an iterative approach is used to solve the linear system. This process is repeated for each section of the manifold along its entire length. Additionally, the program assumes that the coefficient for the upper and lower surfaces of the channel are equal (i.e., h1=h2 and $h_3 = h_4$). The useful heat that is transferred to the air is expressed in termms of the average fluid temperature and the inlet temperature as follows:

$$Q = \Gamma\,(T_f - T_{f,-1}) \tag{22}$$

$$\Gamma = \dot{m}\,C_p/(W\Delta x) \tag{23}$$

Equations (1)-(5) above can be presented in 5×5 matrix form

$$[A] = \begin{bmatrix} A_{11} & h_{1f1} & h_{r12} & 0 & 0 \\ -h_{1f1} & A_{22} & -h_{2f1} & 0 & 0 \\ h_{r12} & -h_{2f1} & A_{33} & h_{2f2} & -h_{r23} \\ 0 & 0 & -h_{2f2} & A_{44} & -h_{3f2} \\ 0 & 0 & h_{r23} & -h_{3f2} & A_{55} \end{bmatrix}$$

$$[T] = \begin{bmatrix} T_1 \\ T_{f1} \\ T_2 \\ T_{f2} \\ T_3 \end{bmatrix} \quad \text{And } [B] = \begin{bmatrix} S_1 + U_L T_a \\ -\boldsymbol{\Gamma}_1 T_{f1,i-1} \\ S_2 \\ \boldsymbol{\Gamma}_2 T_{f2,i-1} \\ -U_b T_a \end{bmatrix} \tag{24}$$

Where

$$[A_{11}] = \left[h_{1f1} + h_{r12} + + U_L\right] \tag{25}$$

$$[A_{22}] = \left[h_{1f1} + h_{2f1} + \boldsymbol{\Gamma}_1\right] \tag{26}$$

$$[A_{33}] = \left[h_{2f1} + h_{2f2} + h_{r12} + h_{r23}\right] \tag{27}$$

$$[A_{44}] = -\left[h_{2f2} + h_{3f2} + \boldsymbol{\Gamma}_2\right] \tag{28}$$

$$[A_{55}] = -\left[h_{3f2} + h_{r23} + U_b\right] \tag{29}$$

The unknown temperatures. T_1, T_2, T_3, T_{f1} and T_{f2} are computed using the Gauss elimination algorithm.

The matrix [A] includes radiative heat transfer coefficients that are dependent on the unknown temperatures. To solve for these unknowns, an iterative substitution technique is applied to each control volume. The theoretical problem of a DPSAH can be solved using the general framework presented in this flowchart. The detailed solution process is illustrated in Figure 3.

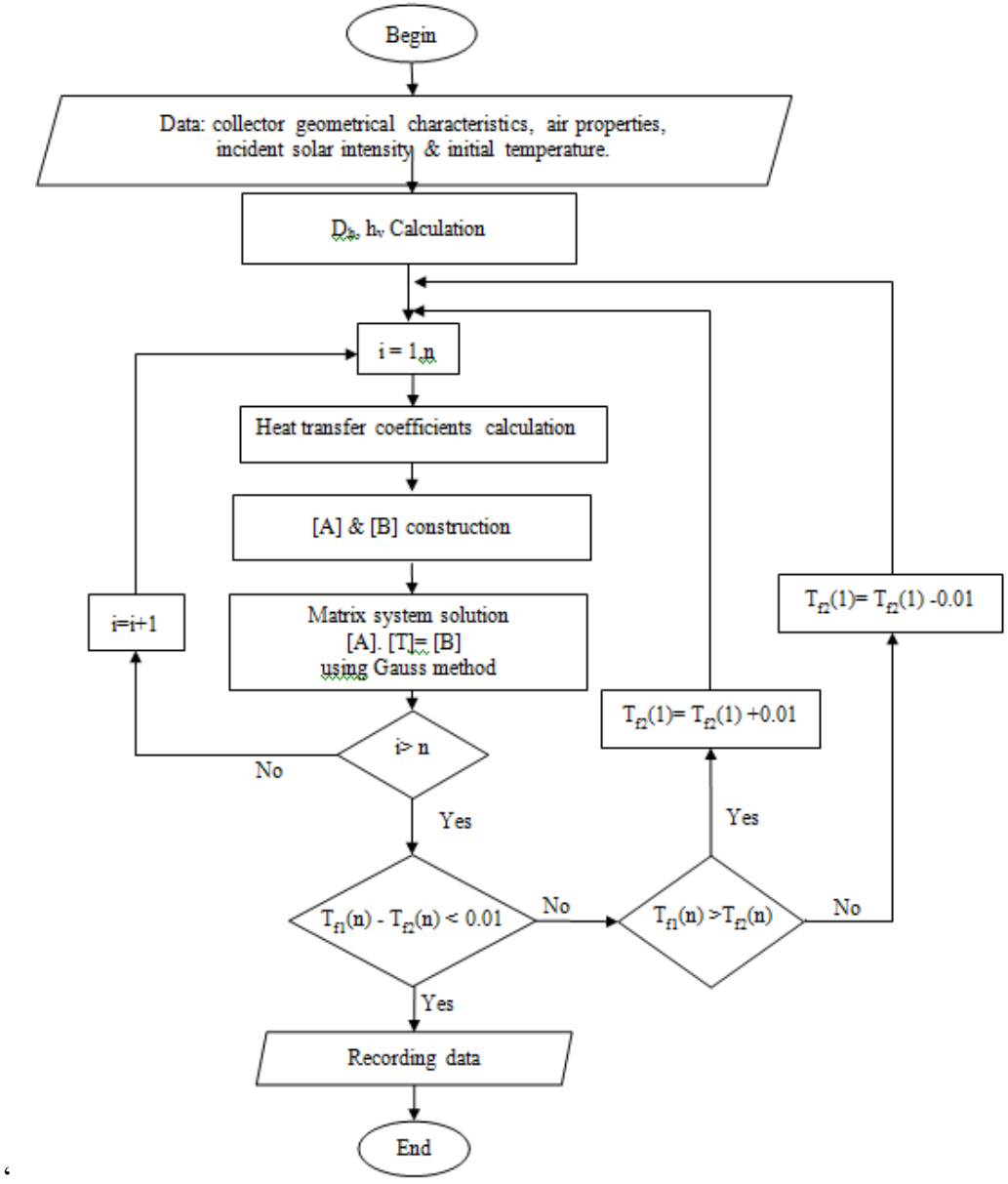


Figure 3. Flowchart for mathematical solution procedure

3. Experimental setup

Figure 1 illustrates a cross-sectional view of DPSAH. The collector is composed of a glass cover, an insulated container, and an absorber made of black-painted aluminum. It measures 1 meter in width and 2 meters in length. Air flows through two channels in this collector, first through the channel created by the glass cover of the absorber plate and then through the channel formed by the bottom plate and absorber. The maximum average radiation that can be achieved is around 950 W/m^2, and dimmers were used to control the amount of radiation the test collector received. The process of data acquisition involved recording various parameters, including the inlet and outlet temperatures, absorber plate and glass cover temperatures, ambient temperature, and the radiation of the solar simulator. In this experiment, a type-k thermocouple was employed, and the temperature at various parts of the DPSAH was recorded after reaching a steady state condition, which occurred approximately 30 minutes after starting the system.

4. Validations

The validation is divided into two parts; the first one is reserved with that found in previous researches as for the second part is devoted to that of our experimental manipulation.

4.1 Validations with literature

To verify the accuracy and dependability of the numerical model employed in this study, we compared the outcomes generated by our code with the findings reported in prior research. Specifically, we analyzed the results presented by Futholi et al. [32] are used to examine the validity of the proposed model from DPSAH for the same configuration. The outlet temperature is shown in Figure 3 as a function of MFR for the same configurations, system characteristics, and operational circumstances (table 1). The comparison results are presented in fig 4 and table1. Figure shown the performance profile of the present model flows the same pace as the experimental of futholi at al [32]. It is clear that the present results are in favorable agreement with the experimental results of Futholi et al.[32]

Table 1. The outlet temperature of the DPSAH for different solar irradiance and MFR (validation of mathematical model with Futholi et al.[32]).

$I_g(w/m^2)$	*Mass flow rate (kg/s)*	*Outlet temperature (°C)*		
		Present result.	*Result of Futholi et al[32].*	*Error %*
425	0.04	42.50	43.5	2.28
	0.06	39.05	40.27	3.01
	0.07	37.07	39.2	5.42
	0.08	36.99	37.7	1.86
	0.09	35.27	36.42	3.14

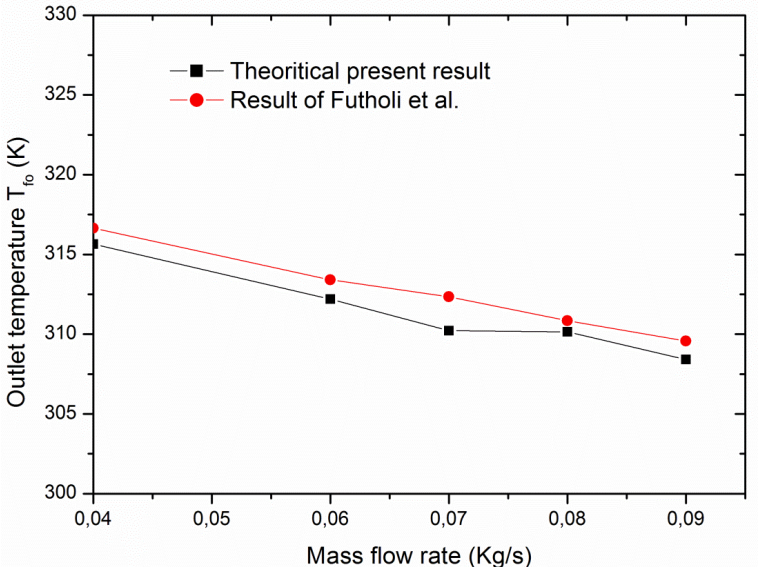


Figure 4. Outlet temperature versus MFR, I=425 watt/m^2

4.2. Validations with experimental data

The validation process involves verifying the accuracy of the mathematical model by comparing the numerical results with the data obtained from experimental testing. This comparison includes evaluating the relative error in the temperatures of the various components of DPSAH, as well as the outlet air temperature. Additionally, the average accuracy of the developed model is assessed.

For a MFR ranging from 0.044 to 0.089 kg/s, the thermal efficiency of the DPSAH varies between 43.07% and 65.32%, with the outlet air temperature ranging from 308.47 K to 316.91 K. These variations are presented in Table 2, which displays the changes in the outlet temperature and the thermal efficiency of DPSAH. It is observed that the thermal efficiency of the DPSAH increases with higher air MFR and solar irradiance.

The comparison presented in Table 2 indicates that the thermal efficiency results produced by the mathematical model exhibit a reasonable level of agreement with the

experimental data, achieving an accuracy of 95.038%. Similarly, the outlet temperature results obtained from the theoretical model demonstrate a high level of accuracy, with a precision of 99.7%.

As can be seen in figure 5, for the temperature of the fluid, the results of the model agree quite well. Figure 6 shows that the temperatures of the glass cover, absorber plate and insulation of the panel obtained from the model reflect a good consistency with those of the experimental for MFR of 0.013 Kg/s. We also showed that the temperature of the absorber plate is the highest, this is due to its coefficient absorption greater than those of the other components.

Table 2. The DPSAH's thermal performance and outlet temperature for various MFR and solar irradiance.

Solar irradiance (w/m^2)	**Mass flow rate (kg/s)**	**Outlet fluid temperature (k)**			**Efficiency %**			**Accuracy %**	
		Theo	**Exp**	**Error %**	**Theo %**	**Exp**	**Error**	**Tfs**	**η**
425	0.044	312.23	311.92	0.10	43.52	43.07	1.04	99.90	98.96
	0.061	310.13	309.44	0.22	50.78	47.3	7.35	99.78	92.65
	0.069	309.44	309.31	0.04	53.46	52.69	1.46	99.96	98.54
	0.078	308.75	308.4	0.12	55.94	55.76	0.32	99.88	99.68
	0.089	308.13	308.47	0.11	59.42	61.92	4.03	99.89	95.97
575	0.044	315.96	316.91	0.30	42.79	45.12	5.16	99.70	94.84
	0.06	313.5	314.16	0.21	49.35	51.56	4.28	99.79	95.72
	0.068	312.57	313.08	0.16	52.08	53.96	3.48	99.84	96.52
	0.076	311.78	313.25	0.47	54.55	61.11	10.73	99.53	89.27
	0.087	310.87	312.37	0.48	57.63	65.32	11.77	99.52	88.23

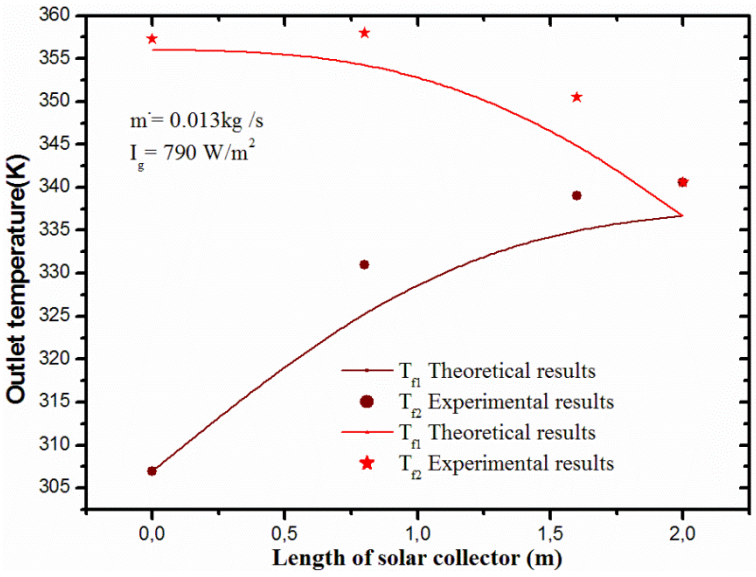


Figure 5. Evolution of the output temperature in relation to DPSAH length

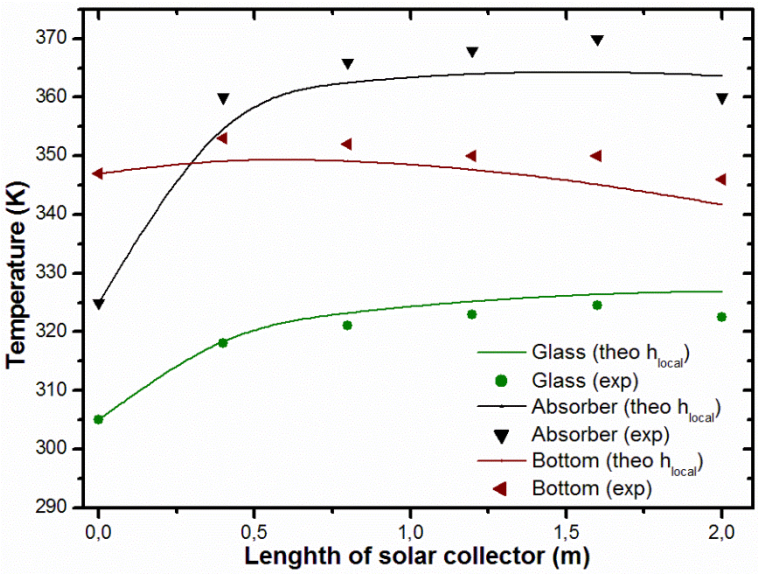


Figure 6. Variations in the panel elements' temperatures according to their length for m = 0.013kg / s, Ig = 790 W / m^2

5. Results and discussions

In this part, a parametric study resides in the representation of the variations of the thermal efficiency and the outlet temperature as a function of the height of the channel at different flow rates and operating modes for a DPSAH. We note from figures 7, that the gradual increase in the height of the channel, causes a drop in outlet temperature and a drop in efficiency. Indeed a fall remarkable output temperature and efficiency for low flow rates compared to at relatively high flow rates. This phenomenon is explained by the fact that the increase in the head at low flow induces a decrease in the exchange coefficient convicted by against in high flow rates, the regime retains its turbulent character which gives a good heat exchange. We refer to figure 7 for L = 2, L=5m and L= 9m where the Nu varies from 5.44 to 33.36 with an solar radiation of 790 W/m^2 shows the drop in temperature from 349.7 to 314.13, from 371.99 to 324.4 and from 380.85 to 335.21 respectively.

From the two figures 8 and 9, it can be seen that the outlet temperature decreases with the increase in the Nusselt number because the amount of air to be heated to overcome the existing amount of heat. This can be explained by the fact that the report of the exchange coefficient on the flow decreases in Nusselt's anointing. To achieve a higher outlet temperature we play on the length of the panel in order to increase the on exchange ace.

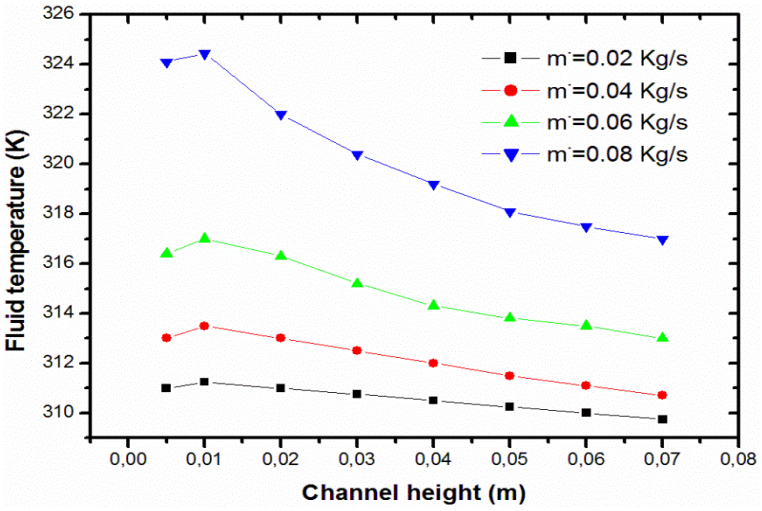


Figure 7. Outlet air temperature variations as a function of height of channel for I=450W/m^2

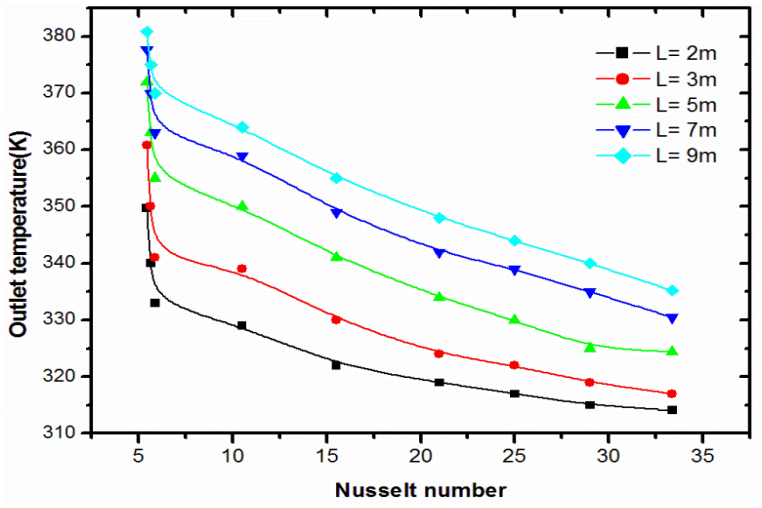


Figure 8. The double pass air collector's outlet air temperature for various Nusselt numbers and collector lengths for I=790(W/m^2).

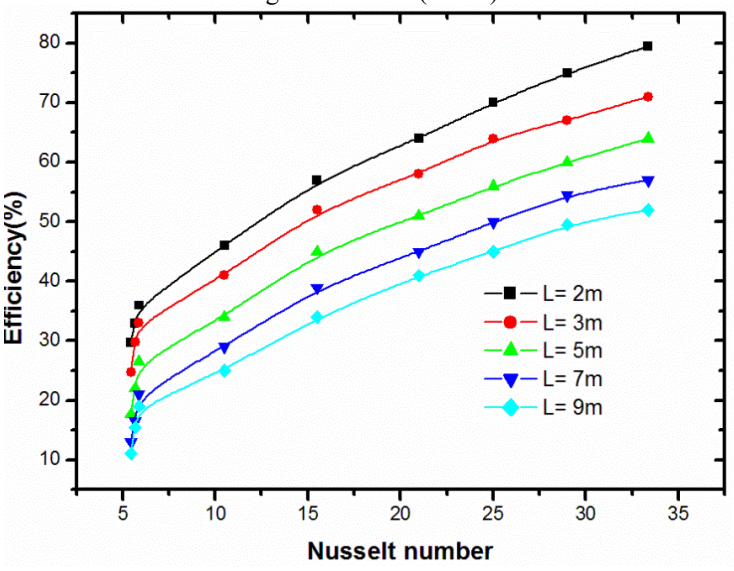


Figure 9. The energy efficiency of DPSAH for different Nu and length of collector at I=790 (W/m^2)

6. Conclusion

This research project examined the efficiency of DPSAH through both theoretical and experimental means. The study focused on determining how MFR and solar irradiance impact the heater's efficiency. To determine the outlet temperature, EBEs were used to derive a steady-state solution. These equations were then applied to each element using thermal balance equations. The developed model was validated against both results from literature and our experimental setup and good agreements were found. The study found that as the Nu increased, the outlet temperature decreased for any solar irradiance. Furthermore, an increase in the Nu led to an increase in energy efficiency. The researchers conducted numerical calculations to analyze temperature distributions for various solar irradiance values. The results of the proposed method closely aligned with the experimentally measured values.

Acknowledgments

This research was funded by the Algerian Ministry of Higher Education and Scientific Research's Directorate General of Scientific Research and Technological Development (DGRSDT) as part of the PRFU project [A11N01UN300120230002].

Nomenclature

T_1	Glass tempertaure (K)
T_2	Absorber plate temperature (K)
T_f	Air flow temperature (K)
T_a	Ambient temperature (K)
T_s	Temperature of sky (K)
I	Incident solar radiation (W/m^2)
h_1	Convective heat transfer coefficient between glass cover and air flow (W/m^{2}K)
h_2	Convective heat transfer coefficient between absorber plate and air flow (W/m^{2}K)
h_{r21}	Radiation heat transfer coefficients between glass cover and absorber plate (W/m^{2}K)
h_{rs}	Radiation heat transfer coefficients between glass cover and sky (W/m^{2}K)
h_w	Heat transfer coefficient of wind (W/m^{2}K)
C_p	Heat capacity of air (J/Kg K)
K_f	Thermal conductivity of air flow (W/m K)
k_{bi}	Thermal conductivity of insulation (W/m K)
U_b	Bottom heat loss coefficient (W/m^2 K)
U_L	Top heat loss coefficient (W/m^{2}K)
$\dot{m}$	Air mass flow rate (Kg/s)
V	Wind velocity (m/s)
Re	Reynolds number
Nu	Nusselt number
L	Length of collector (m)
W	Width collector (m)
X_{bi}	Insulation thickness (m)

d	Spacing between absorber and glass (m)
D_h	Hydrolic diameter (m)
A	Cross section of flow area (m^2)
P	'Wetted perimeter (m)
Q	Heat transferred to the air and can be used.
ε_1	Glass cover emissivity
ε_2	Absorber plate emissivity
α_1	Abrober plate emissivity
τ	Transmissivity
ρ	Density of air stream
σ	Constant of Stefan-Boltzmann
μ	A stream of air's dynamic viscosity

References

[1] P. K. Choudhury and D. C. Baruah, *Solar air heater for residential space heating*, Energy, Ecology and Environment, vol. 2 pp. 387-403, 2017

[2] A. Fudholi, K. Sopian, M. H. Ruslan, M. Alghoul and M. Y. Sulaiman, *Review of solar dryers for agricultural and marine products*, Renewable and sustainable energy reviews, vol. 14 1, pp. 1-30, 2010

[3] N. Wijeysundera, L. L. Ah and L. E. Tjioe, *Thermal performance study of two-pass solar air heaters*, Solar Energy, vol. 28 5, pp. 363-370, 1982

[4] C. Choudhury, P. Chauhan and H. Garg, *Performance and cost analysis of two-pass solar air heaters*, Heat recovery systems and CHP, vol. 15 8, pp. 755-773, 1995

[5] C. Choudhury, P. Chauhan, H. Garg and S. Garg, *Cost—benefit ratio of triple pass solar air heaters*, Energy conversion and management, vol. 37 1, pp. 95-116, 1996

[6] A. Mohamad, *High efficiency solar air heater,* Solar Energy, vol. 60 2, pp. 71-76, 1997

[7] S. Singh, *Thermohydraulic performance of double pass solar thermal collector with inline, staggered and hybrid fin configurations*, Journal of Energy Storage, vol. 27 pp. 101080, 2020

[8] M. M. M. Salih, O. R. Alomar, F. A. Ali and H. M. Abd, *An experimental investigation of a double pass solar air heater performance: A comparison between natural and forced air circulation processes*, Solar Energy, vol. 193 pp. 184-194, 2019

[9] A. Kumar, A. P. Singh and O. Singh, *Performance characteristics of a new curved double-pass counter flow solar air heater*, Energy, vol. 239 pp. 121886, 2022

[10] K. Sopian, M. Alghoul, E. M. Alfegi, M. Sulaiman and E. Musa, *Evaluation of thermal efficiency of double-pass solar collector with porous–nonporous media,* Renewable Energy, vol. 34 3, pp. 640-645, 2009

[11] K. Sopian, W. R. W. Daud, M. Y. Othman and B. Yatim, *Thermal performance of the double-pass solar collector with and without porous media,* Renewable Energy, vol. 18 4, pp. 557-564, 1999

[12] A. Fudholi, K. Sopian, M. Othman, M. Ruslan, M. AlGhoul, A. Zaharim and R. Zulkifly, *Heat transfer correlation for the V-groove solar collector*, Solar Energy Research Institute, University Kebangsaan Malaysia, vol. 43600 pp. 2008

[13] A. Fudholi, M. Ruslan, M. Othman, M. Yahya, S. Supranto, A. Zaharim and K. Sopian, *Collector efficiency of the double-pass solar air collectors with fins*, Presented at Proceedings of the 9th WSEAS international conference on System science and simulation in engineering, pp. 428-434, 2010

[14] A. Fudholi, M. H. Ruslan, L. Haw, S. Mat, M. Othman, A. Zaharim and K. Sopian, *Cost Analysis of Double-Pass Solar Collector with Finned Absorber,* Presented at 9th WSEAS Int. Conf. on Heat and Mass Transfer (HMT'12), pp. 2012

[15] A. Fudholi, M. H. Ruslan, S. Haw, M. Mat, A. Othman, K. S. Zaharim and K. Sopian, *Mathematical model of double-pass solar air collector with longitudinal fins,* Proceedings of the Recent Advances in Fluid Mechanics, Heat & Mass Transfer and Biology, vol. pp. 114-120, 2012

[16] A. Fudholi, K. Sopian, M. H. Ruslan, M. Y. Othman and M. Yahya, *Thermal efficiency of double pass solar collector with longitudinal fins absorbers,* American Journal of Applied Sciences, vol. 8 3, pp. 254, 2011

[17] A. Fudholi, K. Sopian, M. H. Ruslan, M. Y. Othman and M. Yahya, *Analytical and experimental studies on the thermal efficiency of the double-pass solar air collector with finned absorber,* American Journal of Applied Sciences, vol. 8 7, pp. 716, 2011

[18] F. E. Saboya and E. Sparrow, *Experiments on a three-row fin and tube heat exchanger,* J. Heat Transfer;(United States), vol. 98 3, pp. 1976

[19] S.-Y. Yoo, H.-K. Kwon and J.-H. Kim, *A study on heat transfer characteristics for staggered tube banks in cross-flow*, Journal of Mechanical Science and Technology, vol. 21 pp. 505-512, 2007

[20] C.-H. Huang, I.-C. Yuan and H. Ay, *A three-dimensional inverse problem in imaging the local heat transfer coefficients for plate finned-tube heat exchangers,* International Journal of Heat and Mass Transfer, vol. 46 19, pp. 3629-3638, 2003

[21] A. H. Benmachiche, C. Bougriou and S. Abboudi, *Inverse determination of the heat transfer characteristics on a circular plane fin in a finned-tube bundle*, Heat and mass transfer, vol. 46 11-12, pp. 1367-1377, 2010

[22] N. Moummi, S. Youcef-Ali, A. Moummi and J. Desmons, *Energy analysis of a solar air collector with rows of fins,* Renewable Energy, vol. 29 13, pp. 2053-2064, 2004

[23] F. Aissaoui, A. H. Benmachiche, A. Brima, D. Bahloul and Y. Belloufi, *Experimental and theoretical analysis on thermal performance of the flat plate solar air collector*, International Journal of Heat and Technology, vol. 34 2, pp. 213-220, 2016

[24] F. Aissaoui, A. H. Benmachiche, A. Brima, Y. Belloufi and M. Belkhiri, *Numerical study on thermal performance of a solar air collector with fins and baffles attached over the absorber plate*, International Journal of Heat and Technology, Vol. 35, No. 2, pp. 289-296.

[25] F. AISSAOUI, *Contribution à l'étude de transfert de chaleur d'un capteur solaire placé dans un climat aride: cas de la région de Biskra*, PhD Thesis, Université Mohamed Khider-Biskra, 2017

[26] K. Ong, *Thermal performance of solar air heaters—Experimental correlation*, Solar Energy, vol. 55 3, pp. 209-220, 1995

[27] G. A. Hawkins, Heat Transmission. William H. McAdams. McGraw-Hill, New York-London, ed. 3, 1954. xiv+ 532 pp. Illus. $8.50, Science, vol. 120 3128, pp. 984-984, 1954.

[28] M. D. Bazilian and D. Prasad, *Modelling of a photovoltaic heat recovery system and its role in a design decision support tool for building professionals,* Renewable Energy, vol. 27 1, pp. 57-68, 2002

[29] J. A. Duffie and W. A. Beckman, *Solar engineering of thermal processes*, John Wiley & Sons, Inc. New York, vol. pp. 1991

[30] W. C. Swinbank, *Long-wave radiation from clear skies*, Quarterly Journal of the Royal Meteorological Society, vol. 89 381, pp. 339-348, 1963

[31] G. N. Tiwari, *Solar energy: fundamentals, design, modelling and applications,* Alpha Science Int'l Ltd., 2002

[32] A. Fudholi, K. Sopian, M. H. Ruslan and M. Y. Othman, *Performance and cost benefits analysis of double-pass solar collector with and without fins,* Energy conversion and management, vol. 76 pp. 8-19, 2013